Martensite transformation kinetics and microstructural evolution during quench and partitioning process of high aluminium medium carbon steel

Vinod Kurup[1*], *Charles* Siyasiya[1] , and *Roelf* Mostert[1]

[1] Department of Material Science and Metallurgical Engineering, University of Pretoria, South Africa

Abstract. The quench and partition process was studied in a high aluminium (Al) medium carbon (C) steel by varying the quench temperature which is one of the process parameters The first part of the paper deals with modelling athermal martensite transformation using an empirical approach. This model is an improvement on Koiestein and Marburger's model, and it better represents the martensitic transformation. The second part of the paper deals with microstructure evolution in high Al steel when subjected to the quench and partition process. The maximum retained austenite (RA) obtained was 13% at a quenching temperature of 260 ºC. The addition of Al promoted the formation of bainite during the partition stage

1 Introduction:

Advanced high strength steels (AHSS) are a significant driver in developing new steels for automotive applications. The quench and partitioning process (Q&P) proposed by Speer et al. [1] is one such process that promotes the development of third-generation AHSS [2]. In general, the Q&P process involves austenitization followed by the first quench to a temperature below M_s, at which austenite transforms to martensite (α') leaving some austenite (γ) untransformed. Subsequent to this, is the partitioning step where the sample is held at the same quench temperature or heated to higher temperature where the carbon (C) partitions from α' to γ and enriching the γ phase. Depending on the carbon content, the enriched γ phase remain stable at room temperature (RT) or is partially transformed to fresh martensite α'_f on further quenching to RT after the partitioning step.To ensure carbon partitions from α' to γ other competing products like cementite and carbides are prevented by adding silicon [3,4]. The addition of silicon (Si) stabilizes the γ by inhibiting the carbide precipitation due to silicon's low solubility in carbide [5]. Elevated Si levels result in the formation of a stable oxide layer which prevents the formation of an inhibition layer during the hot-dip galvanizing process leading to surface finish issues [6].

To mitigate this, the partial or complete substitution of Si is required, and aluminium (Al) has been found to fit this purpose based on studies on TRIP steel [7,8]. In the present study, Si is partially replaced by Al, and the alloy is subjected to Q&P heat treatment. The quench temperature, one of the variables, is varied to see its effect on the amount of retained austenite (RA)

*vinod.kurup@up.ac.za

2 Material and Methodology

The chemical composition of the steel used in the present study is listed in Table 1 and designated as alloy1. This alloy was induction melted and cast. The cast ingot was reheated to 1200℃ for 3 hours, followed by hot forging at 900℃ to produce a 50 mm square bar. This was further hot rolled into 15 mm diameter and 30 mm long rods. The specimens of 5 mm diameter and10 mm length were wire cut out from the rods for dilatometer experiments. Heat treatments were carried out in Bähr 805A dilatometer. Samples were placed between silica pushrods and heated using an induction coil, and helium was used as a quenching medium. Three sets of heat treatments were carried out as follows

a. Critical temperatures Ac_1 and Ac_3 of were determined by heating the samples to 650℃ at 10℃/s and heated further to 950℃ at 0.0001℃ /s before cooling down to RT
b. To determine the Ms temperature, the sample after austenitization at 950℃ was quenched to RT at 100℃ per sec. The data obtained from the dilation was used to determine M_s and the athermal kinetics of martensitic transformation.
c. Two-step Q&P heat treatment was done by varying the quench temperatures above and below the calculated optimum temperature (OPT). The quench temperatures were 180,200 and 215,220℃ (below OPT) and 240 and 260℃ (above OPT).

The critical temperatures are listed in Table 1 and the schematic of two- step Q&P process is shown in Figure 1

Table 1 : The chemical composition (in Wt %) and the critical temperature of the steel alloy

Element	C	Mn	Si	Al	Cr	P	S	M_s	Ac_1	Ac_3
Amount (Wt. %)	0.25	2.9	0.62	1.68	0.47	0.011	0.014	380°C	700°C	910°C

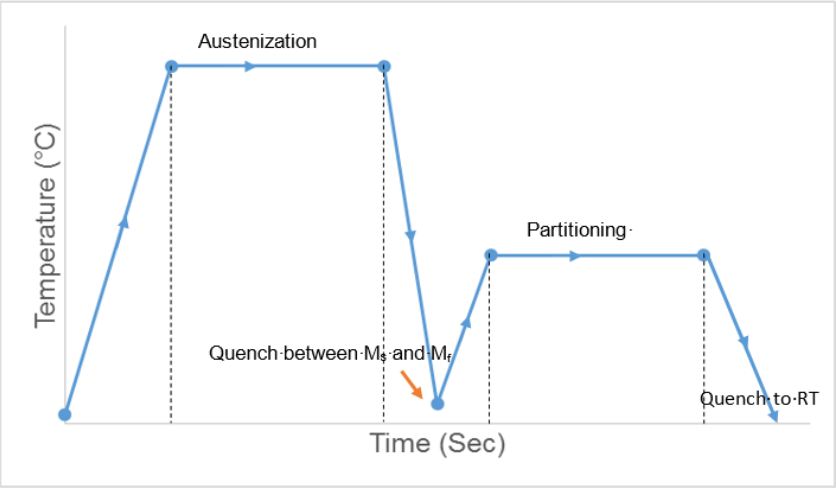

Figure 1: Schematic diagram of the two-step quench and partitioning heat treatment

The heat-treated samples were analyzed using neutron diffraction at the Nuclear Energy Council of South Africa (NECSA). The purpose was to identify the presence of different phases, mainly RA and its volume fraction, after subjecting the samples to a two-step Q&P process. The samples were scanned in the 2θ range from 27 to 115 degrees. The diffraction patterns obtained were analyzed by TOPAZ 4.2 software using the Reitveld method [9] to determine the volume fraction of phases and the corresponding lattice parameters. Using the empirical relationship between lattice parameter of austenite a (γ)and composition [10] as given in equation 1, the carbon content of RA was determined.

$$a\,(\gamma)=0.3556+0.00453w_c+0.00095w_{mn}+0.00056w_{al}+0.0006w_{cr}-0.0002w_{ni} \quad (1)$$

The heat-treated samples were ground and polished to obtain a metallographically polished surface, which was etched with 2% nital to reveal the microstructure using a scanning electron microscope (SEM). Thin foil samples were prepared for transmission electron microscopy (TEM) and transmission kikuchi diffraction (TKD) analysis. Disc samples 3 mm in diameter and 0.1 mm in thickness were wire cut and ground to 50μm. The jet polishing was carried out using the TENUPOL-5 apparatus. The electrolyte mixture of 5% perchloric acid and 95% glacial acetic acid was used, and the apparatus was operated at -15℃. The jet polishing parameters were set at flow rate=35ml/s; voltage of16 to-21 V; current of 28 mA. These samples were also used for TKD to determine the RA distribution in the microstructure. TEM was carried out using the JEOL 2100 LaB_6 operated at 200 KV.

3. Results:

3.1 Athermal martensite formation and transformation rate:

Martensite forms during the first quench step in the two-step Q&P heat treatment. Knowing the volume fraction of martensite present at each quench temperature is essential, as it is one of the variables for the Q&P process. The dilation data obtained from quenching the steel was used to calculate the fraction of martensite as a function of temperature by applying the lever rule. The transformation kinetics of athermal martensite depends on the degree of supercooling and is captured by the model proposed by Koistinen-Marburger (K-M model).

$$f_m = 1 - exp\,(-\alpha(M_s - T) \quad (2)$$

Where f_m is the martensite fraction, α is the transformation rate parameter, M_s is the martensite start temperature, and T is the quench temperature.

The rate parameter α is assumed to be 0.011 for iron-carbon alloys and steels. For the present material, a nonlinear behaviour was observed in the plot of ln (ln (1/ (1- f_m)) vs. ln (Ms-T) as shown in Figure 2(b). It shows two linear segments at the beginning and end of martensitic transformation and a transition stage. This requires improvement in the K-M model. The modified form of the original K-M equation was proposed by Lee and Tyne [11].

$$f_M = 1 - exp\,(-\alpha(Ms - T))^{\beta} \quad (3)$$

Where β is used to control the slope of the linear part of the curve as in Figure 2(b).

The α parameter as a function of temperature shown in Figure 2(c) is not constant. Therefore, it is fitted with a double exponential equation as a function of temperature as given in Equation 4[12].

$$\alpha = \alpha_0 + \Delta\alpha \, exp(-exp\, K_m\,(T - T_o)) \qquad (4)$$

Where α_0 is the minimum of α; $\Delta\alpha$ is the amplitude of the curve; $T_o$is the temperature where the maximum transient rate occurs in the martensitic transformation curve in figure 2(a). K_m controls the transient rate in Figure 2(c) and is optimized by the least square method. Figure 2(d) shows modified K-M equation fits the experimental values with better accuracy. The optimized parameters for Equations 3 and 4 are shown in Table 2

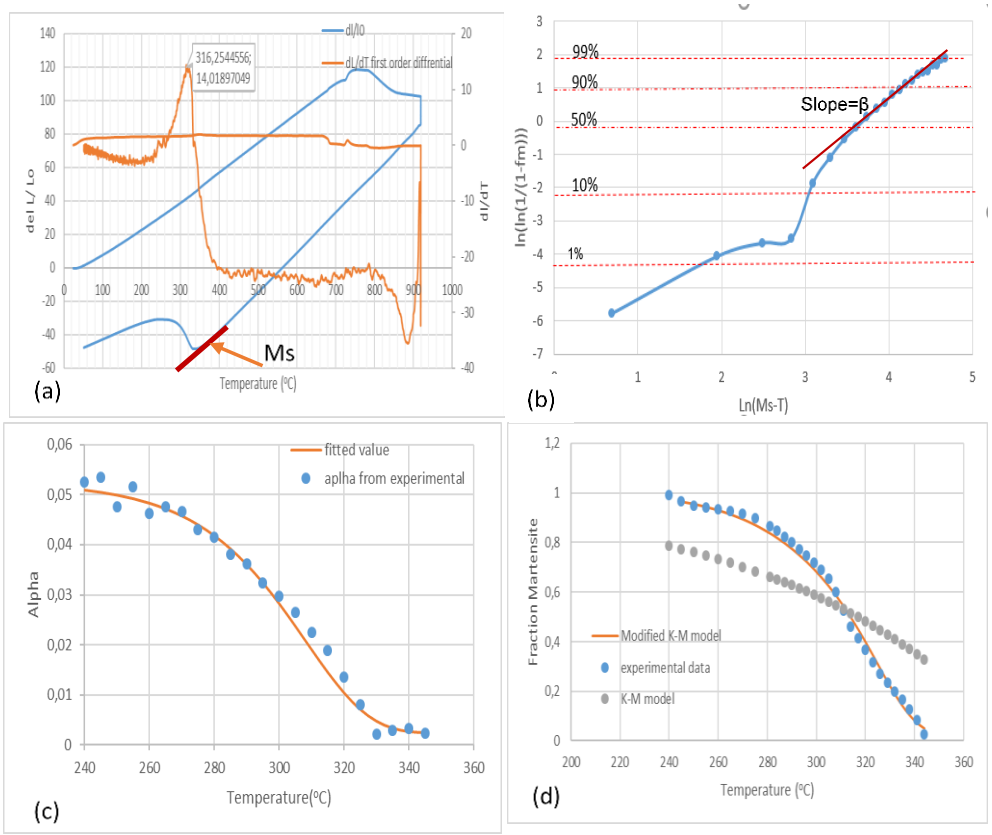

Figure 2: (a) Determination of the M_s using the dilatometer (b) Plot of ln(ln(/1-fm) vs. ln(M_s-T) showing a nonlinear behaviour (c) Plot of α parameter against temperature with nonlinear fitting; (d) Comparison of athermal martensite transformation obtained from dilatometer fitted with modified K-M equation and K-M model plot.

Table 2: Optimized fitting parameter for martensite transformation

α_0 [°C^{-1}]	$\Delta\alpha$[°C]	k_m [°C^{-1}]	T_0 [°C]	β
0.00431	0.0095	0.0813	316.25	1.929

3.2 Dilatometry of two-step Q&P process

The optimum quench temperature (OQT) using the Speer model with constrained carbon equilibrium (CCE) [1] was determined as 230℃ with the RA content being 0.19 volume fraction. The typical dilation curve for a two-step Q&P process (260℃ quench temperature (QT)-400℃ partitioning temperature (PT) for 200 s) is shown in Figure 3(a).

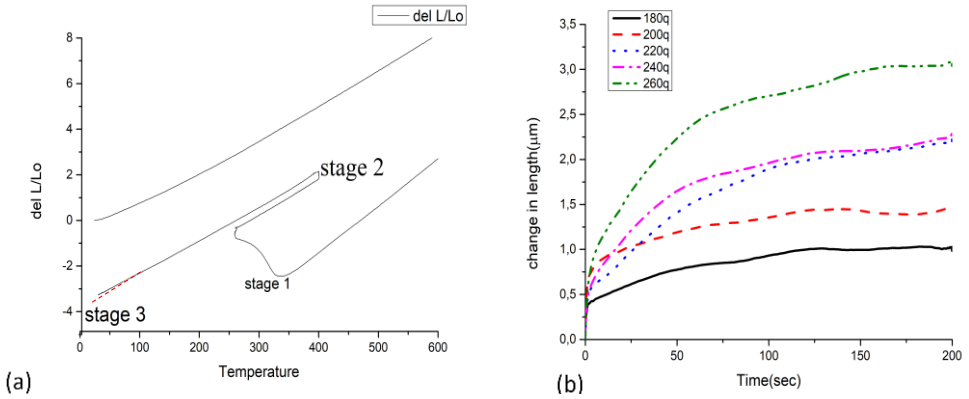

Figure 3: (a) Partial dilation curve showing different stages of Q&P process (b) Net change in length at a partitioning temperature of 400℃ corresponding to different quench temperature

The microstructure evolution during the Q&P process involves three stages, as shown in Figure 3(a). Stage I shows a sharp increase in dilation due to α' formation at M_s and continues until QT=260℃. Since the QT is between M_s and M_f, we find that some austenite remains untransformed. During heating from QT to PT=400℃, we see a linear increase. In stage II of the Q&P process, during the isothermal hold at 400℃, we see an increase related to carbon partition from martensite to untransformed austenite, carbide formation, and bainite transformation. These three processes overlap, so it is difficult to differentiate them. The net expansion during stage II at various quench temperatures is shown in Figure 3(b), with quench temperatures above and below the calculated OPT. During stage III, when the sample is quenched to RT after the partitioning treatment, the RA will partially transform to fresh martensite if the M_{s2} of the RA is higher than RT (M_{s2} is the M_s temperature of the carbon-enriched austenite). In Figure 3(a) in stage III, we see a slight deviation from linearity, indicating the formation of fresh martensite.

3.3 Neutron diffraction

The neutron diffraction results of samples quenched at different QT are shown in Figure 4. As the QT increases, the amount of RA increases, unlike predicted by Speer, where RA decreases after the OPT. This is evident from the increase in the intensity of the austenite

peaks. The amount of RA from the neutron diffraction analysis using the Reitveld method is shown in Table 3. The RA value is maximum at 260 QT with a 12.9 % volume fraction. The lattice parameter and the carbon content of RA decrease as the QT increases.

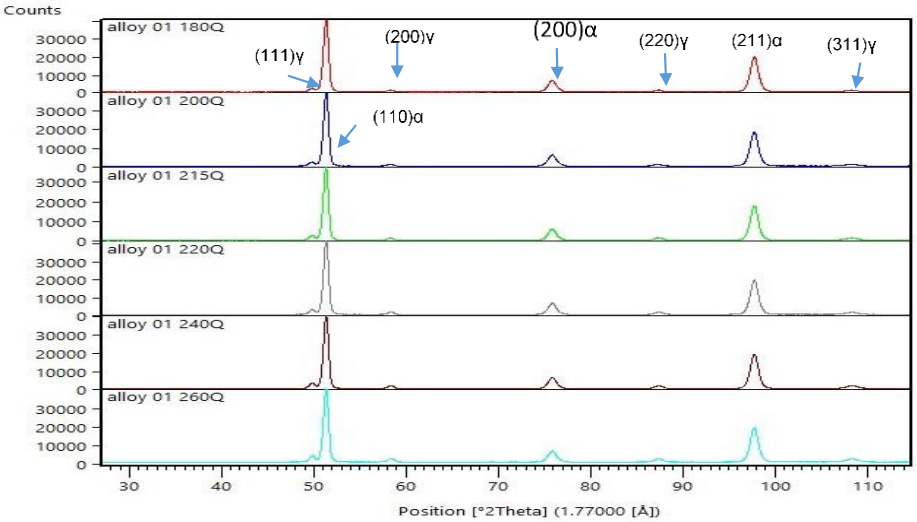

Figure 4 : Neutron diffraction pattern of Q&P samples at various QT showing presence of retained austenite

Table 3 : Quantitative results estimated from Rietveld analysis of the neutron diffraction data

Quench Temp	% RA	Lattice parameter(Å)	%C
180	7,8	3,5975±0.0004	0,64
200	8,5	3,5975±0.0002	0,64
215	10,4	3,5947±0.0003	0,58
220	10,1	3,5946±0.0003	0,57
240	11,9	3,594±0.0003	0,56
260	12,9	3,5903±0.0003	0,54

3.4 Microstructural analysis:

The microstructures obtained from a two-step Q&P process at selected QTs are shown in Figure 5. At QT=180℃, the sample showed martensite ($\acute{\alpha}$), tempered martensite (TM), and bainite (B). Tempered martensite was from the martensite formed after the first quench, which is tempered during the partitioning stage. Fresh martensite formed from the RA that had higher carbon content. The 220 QT sample showed coarser and ridge-like laths corresponding to tempered and untempered martensite, Figure 5b. Small blocky regions with irregular morphology correspond to the bainite phase. The 240 QT sample shows ridge-like

laths and tempered martensite with clear carbide precipitated within the lath, Figure 5c. The 260 QT sample shows a significant amount of bainite in the microstructure, Figure 5d.

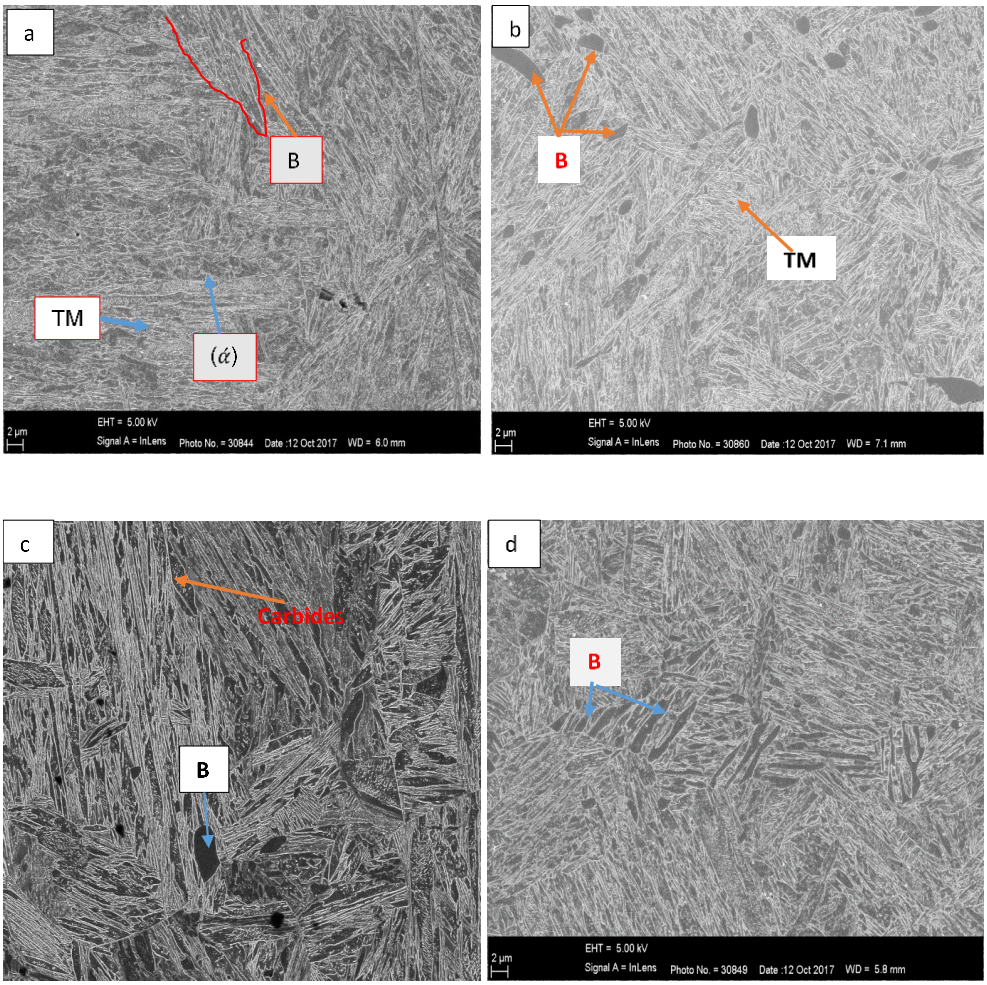

Figure 5: SEM micrographs of samples quenched at different temperatures (a) 180 ºC (b) 220 ºC (c) 240 ºC and (d) 260 ºC and partitioned at 400ºC for 200 seconds and then quenched to room temperature. All micrographs were taken at a magnification of 5000X.B=Bainite; (ά)=martensite;TM tempered martensite

Samples were also quenched at 230℃, which is the OQT for this alloy, and partitioned at 325℃ in a salt bath furnace for TEM and TKD analysis. The TEM image showed the presence of thin laths of retained austenite, as shown in Figure 6. The dark field image and its diffraction establish the existence of austenite inform of thin laths. The TKD image in Figure 7 shows the distribution of austenite in the form of film and blocks. It also revealed the presence of epsilon carbides and cementite in the martensite lath. There were some regions with zero solution in the phase-contrast map, which could have been fresh martensite and, due to its high dislocation density, cannot be resolved, or thin austenite films whose size was less than the resolution limit of 50 nm.

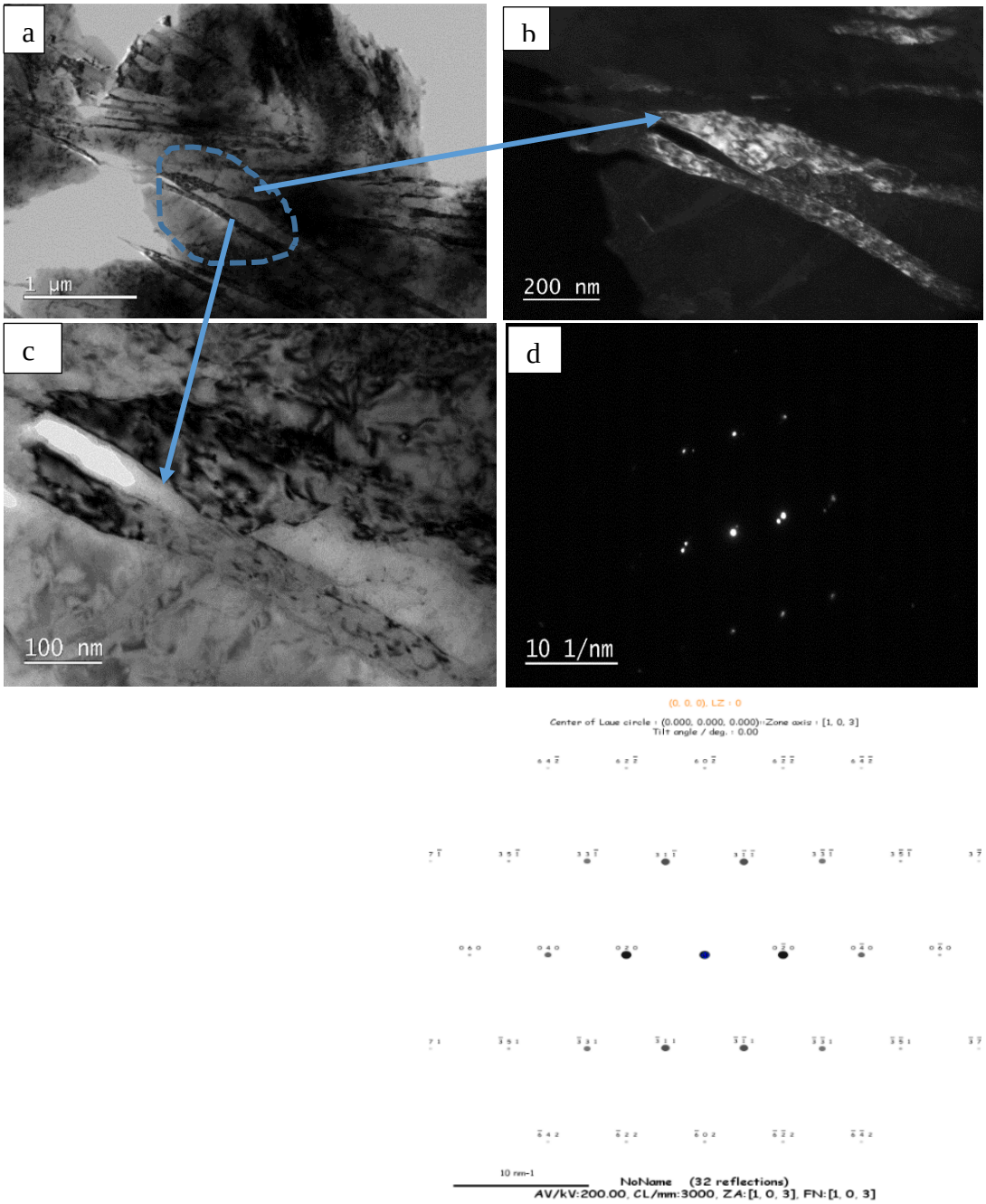

Figure 6: TEM image of alloy1 subjected 230ºC quench and partitioning at 325ºC. a) General area image b) bright-field image c) dark field image d) SAED of austenite with [1 0 3] zone axis

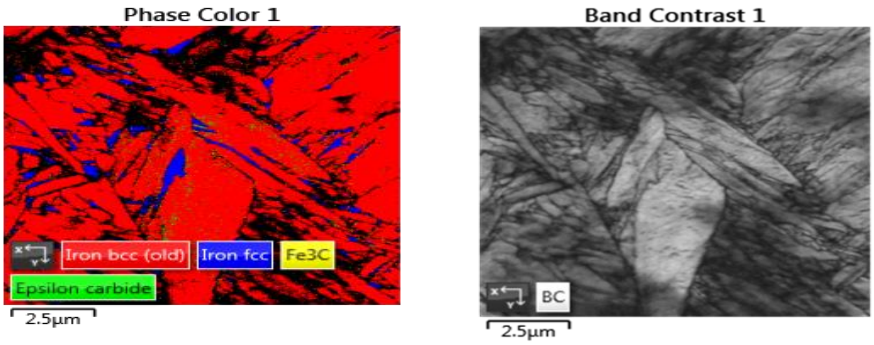

Figure 7: Phase colour map and band contrast of sample quenched at 230 ºC and partitioned at 325 ºC, showing the presence of retained austenite and carbides

4. Discussion:

Athermal martensitic transformation during stage I of two-step Q&P was modelled using a modified K-M equation. This was done because the ln (ln (1/1-fm)) vs. ln (Ms-T) plot was not linear, as one would expect from the K-M equation. There are other models that describe athermal martensitic transformation (a) Van Boheman and Sietsma model (V-S model) [12] and (b) Van Bohemen model (V model) [13]. Both models incorporate the dependence of chemical composition on martensitic transformation and are said to be better in predicting martensitic transformation in low alloy steels. The V model is an improvement of the V-S model to include high carbon steel. Both models also have a linear relationship between the rate parameter α and the composition of the alloy. In this case, these models could not be used because of the high percentage of aluminium content, which is not considered in both the V-S and V models. Moreover, the α seems to be a non-linear function of temperature, as seen in Figure 2(c), which fits best with a double exponential function of temperature. Once the martensitic transformation rate is correctly fitted, it can be used in the Speer model [1] to predict the maximum RA at a given temperature, Figure 8.

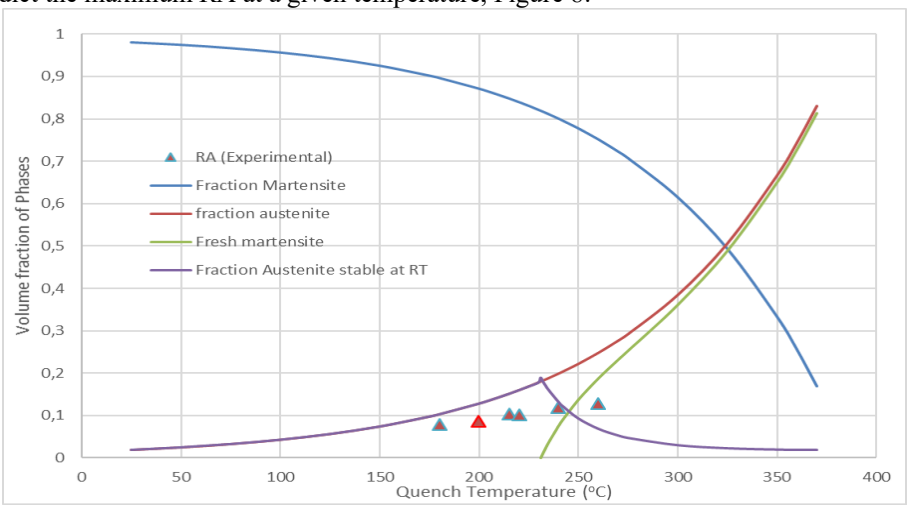

Figure 8: Calculated phase fraction as a function of quench temperature for the alloy with high Al. The fraction martensite and austenite correspond to the fraction of martensite and retained austenite present after the initial quench. "Fresh martensite" is the fresh/secondary martensite formed after the partitioning step. "Fraction austenite stable at RT" refers to austenite present after the second quench.

The RA determined from the neutron diffraction at various QT's denoted as RA (experimental) in Figure 8 seems to be lower than predicted by the Speer model [3]. This is due to the CCE condition assumed in the Speer model, where the carbon is allowed to partition between phases, and other competing reactions are suppressed.[1]. As seen from SEM images, carbides were present in martensitic lath, and the presence of bainite was observed in all samples at various QTs. Thus, the carbon available for RA stabilization was less; hence, the volume fraction of RA was lower than predicted by the Speer model. The carbon content RA was found to be higher than the initial carbon content of the alloy, which signifies the partition of carbon from $\acute{\alpha}$ to RA.

The sample quenched at 260 ℃ exhibited a maximum RA of 13%. The examination of the partition stage at 260, as seen in Figure 3(b), showed maximum expansion. This expansion could be attributed to bainite formation as net expansion due to carbon partitioning is small [15]. The microstructure in Figure 5(d) also shows more bainite. Aluminium addition seemed to promote bainite formation, and it was observed in all the samples quenched at different temperatures though the amount was higher at higher QT. This was due to aluminum's ferritizing effect, which increases the bainite nucleation's driving force [16]. When the bainite subunit forms, it ejects carbon to the austenite, thus temporarily stabilizing the austenite. If the carbon is diffused away or carbon is removed by carbide formation, more bainite subunits form. At higher temperatures, carbon diffusion is higher, thus, leading to more bainite nucleation. The purpose of adding aluminium is to retard carbide formation, but as seen from TKD images in Figure 7, epsilon carbide is not completely avoided, which can promote bainite phase formation. Thus bainite formation leads to austenite stabilization by carbon enrichment. The remaining austenite regions left after bainite formation in the form of thin films are stabilized, as seen in TKD and TEM images.

5. Conclusion:

- The K-M model for athermal martensitic transformation is modified by characterizing the alpha parameter's evolution with temperature and fitting well with the experimentally observed martensite fraction data.
- The maximum retained austenite observed in high Al medium carbon steel was 13% at 260 ºC, less than the Speer model prediction. This is related to bainite formation as addition aluminium promotes bainite formation.

Acknowledgment: The authors would like to acknowledge Ferrous Metal Development Network (FMDN) for the financial support. The authors also want to acknowledge NECSA and NMMU for neutron diffraction and TEM analysis.

References:

1. J.Speer,D K Matlock ,B C De Cooman,J G Schroth Acta Mater.;**51**(9):2611–22. (2003)
2. .D.E Matlock.,V.G Bräutigam,.J. Speer. Vols. **426**–432, Materials Science Forum.. 1089–1094 p.(2003)
3. J.G Speer , F.C Rizzo,D.K Matlock, D.VEdmonds. Mat. Res **8**(4):417–23. (2003)
4. D.T Pierce ,D.R Coughlin, D.LWilliamson, K.D.Clarke, A.J Clarke, J.G Speer , et al. Acta Mater **90** ;417-430 (2015)
5. N Lim, H Park, S Kim,C Park. *Effects of aluminum on the microstructure and phase transformation of TRIP steels*. Met Mater Int.;**18**(4):647–54. (2012)
6. Y Sakuma, O Matsumura, H Takechi. *Mechanical properties and retained austenite in intercritically heat-treated bainite-transformed steel and their variation with Si and Mn additions*. Metall Trans A;**22**(2):489–98. (1991)
7. P.J Jacques,E Girault , A Mertens ,B Verlinden ,J van Humbeeck,F Delannay ; ISIJ Int. ;**41**(9):1068–74. (2001)
8. J Mahieu, B C De Cooman,J Maki, S Claessens . *Hot-dip galvanizing of Al alloyed TRIP steels.* Iron Steelmaker.;**29**(6):29–34. (2002)
9. W.I.F David . Powder diffraction: Least-squares and beyond. J Res Natl Inst Stand Technol;**109**107-123;(2004)
10. N H van Dijk,A.M Butt,L Zhao ,J Sietsma ,S.E Offerman, J.P Wright, et al. *Thermal stability of retained austenite in TRIP steels studied by synchrotron X-ray diffraction during cooling*. Acta Mater;**53**(20):5439–47. (2005)
11. S.J Lee , C.J.Van Tyne.. Metall Mater Trans A ;**43**(2) (2012)
12. S.Kim , J Lee ,F Barlat, M.G Lee.. Acta Mater.;**109**:394–404. (2016)
13. S.M.C van Bohemen , J Sietsma .. Mater Sci Technol.;**25**(8):1009–12.(2009)
14. S.M.C van Bohemen . *Bainite and martensite start temperature calculated with exponential carbon dependence*. Mater Sci Technol;**28**(4):487–95. (2012)
15. M.J.Santofimia ,L Zhao ,J Sietsma . **706–709**, Materials Science Forum.. p. 2290–5. (2012)
16. A Mertens , P.J Jacques ,J Sietsma , F Delannay . Steel Res Int .**79**(12):954–9.(2008)